An Evaluation of CO_2 Laser Beam Welding on a Ti_3Al-Nb Alloy

Laser beam welding of a Ti-14Al-21Nb alloy produced rapid cooling rates that promoted more ductile weld microstructures than those produced using arc welding processes

BY G. S. MARTIN, C. E. ALBRIGHT AND T. A. JONES

ABSTRACT. The CO_2 laser beam weldability of Ti-14.3 wt-% Al-21 wt-% Nb, a Ti_3Al-Nb (alpha$_2$ aluminide) alloy, was investigated. A sequence of pulsed and continuous wave (CW) CO_2 laser beam welds was made on 1.7-mm (0.067-in.) thick coupons of Ti-1421. The weld cross-sections were subjected to microhardness evaluation and characterized hy optical metallography. The hardness values were plotted with respect to calculated cooling rates to reveal possible trends in microhardness.

Laser welds were produced without cracks, porosity or other discontinuities. Laser welding with calculated cooling rates between 195° and 10,400°C/s produced relatively constant microhardness values. These values ranged between 373 and 432 DPH for the heat-affected zone (HAZ), and between 364 and 416 for the fusion zone (FZ). These results are in contrast to Mascorella's results for gas tungsten arc welding, which showed microhardness values have an increasing trend with increased cooling rate (from 297 to 488 HAZ and from 292 to 459 FZ for cooling rates from 2 to 50°C/s)

Bend ductility values within the unaffected base metal (UBM) range were obtained in full penetration longitudinal bend specimens for laser welds with calculated cooling rates above 3400°C/s. For cooling rates of 1380°C/s and lower ductilities were well below the UBM range.

The slower cooled welds exhibited a larger flat cleavage fracture area and lower ductility than the rapidly cooled welds.

The results of this investigation show that careful selection of CO_2 laser welding conditions will result in cooling rates that will yield more ductile HAZs and FZs when compared to gas tungsten arc welding (GTAW).

G. S. MARTIN is with General Electric Corp., Cincinnati, Ohio. C. E. ALBRIGHT is with Department of Welding Engineering, Ohio State University, Columbus, Ohio. T. A. JONES is with Ford Motor Co., Dearborn, Mich.

Introduction

The demands for higher performance military gas turbine engines require materials with lower density and higher operating temperature capabilities than are available in common aerospace alloys. Ti-14 wt-% Al-21 wt-% Nb, designated hereafter as Ti-1421, exhibits attractive strength, creep and elastic modules properties, and has a lower density than conventional titanium alloys (Ref. 1). The low-density ordered matrix structure of Ti-1421 exhibits elastic modules at elevated temperature comparable to that of nickel-based superalloys (Ref. 2). Replacement of the denser nickel-based superalloys with Ti-1421 would allow similar overall engine performance and a considerable weight reduction.

Sheet product forms of alpha-beta titanium alloys for aerospace applications normally exhibit a fine equiaxed alpha grain structure that is a result of high-temperature rolling in the alpha phase field. This process is commonly known as alpha-beta processing. Fusion welding greatly modifies this structure. The solidified fusion zone (FZ) structure and heat-affected zone (HAZ) structure is completely different from that of the unaffected hase metal UBM. These two zones typically exhibit higher strength and lower ductility than the UBM. This occurs because the fast cooling rates experienced in the alpha phase temperature field in both the FZ and the HAZ produce martensitic and/or Widmanstätten alpha. Both of these structures exhibit higher strength and lower ductility than the finely equiaxed alpha UBM. Another detractive feature of the FZ-HAZ microstructure is the large prior beta grain size that results from the typically high heat inputs associated with arc fusion

KEY WORDS

Ti_3Al-Nb Alloy
Cooling Rates
Ductility
Microhardness
Laser Welding
Titanium Aluminides
Intermetallics
Ti-1421
Fractography

Table 1 — Chemical Composition of Ti-1421 Sheet

Element	Weight-%	Atom-%
Al	14.800	26.00
Nb	21.300	10.80
Fe	0.065	0.05
O	0.058	0.20
N	0.006	0.02
Ti	bal	bal

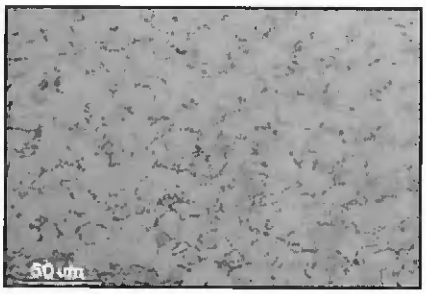

Fig. 1 — Light micrographs of the as-received Ti-1421 sheet material.

Table 2 — CO_2 Laser Variables and Identification Numbers for Microhardness Test

Power Watts	Pulsed[a] or CW	Velocity in./min[c]	Cooling Rate, °C/s	Weld No.	No. RPT[b]	Full Weld
650	CW	3	371	70701	3-D	no
650	CW	7	3, 476	70703	3-D	no
650	CW	9	4, 965	70704	3-D	no
650	CW	10	195	70706	2-D	yes
650	5ms/13ms	10	195	70709	2-D	yes
650	CW	11	5, 937	70705	3-D	no
650	3ms/6ms	20	1, 384	70707	2-D	no
1000	CW	25	451	70502	2-D	yes
1000	10ms/20ms	50	2, 880	62806	2-D	yes
1000	CW	50	3, 021	70501	2-D	yes
1000	1ms/2ms	50	3, 021	62802	2-D	yes
1000	5ms/10ms	50	3, 021	62804	2-D	yes
1000	CW	75	3, 470	42436	2-D	yes
1000	5ms/10ms	100	11, 279	62803	2-D	no
1000	1ms/2ms	100	11, 279	62801	2-D	no
1000	CW	100	11, 279	42435	2-D	yes
1000	10ms/20ms	100	11, 279	62805	2-D	yes
1000	CW	125	24, 966	42434	2-D	no
1000	CW	150	34, 306	42433	2-D	no
1000	CW	75	37, 306	42432	3-D	no
1000	CW	200	41, 246	42431	3-D	no
1400	CW	125	6, 346	42426	2-D	yes
1400	CW	150	6, 563	42425	2-D	no
1400	CW	175	13, 363	42424	3-D	no
1400	CW	200	17, 321	42423	3-D	no
1550	6ms/8ms	150	8, 058	70301	2-D	yes
1600	CW	40	1, 294	70320	2-D	yes
1600	CW	50	2, 112	70319	2-D	yes
1600	CW	75	2, 860	70318	2-D	yes
1600	CW	100	4, 282	70317	2-D	yes
2000	CW	75	2, 238	70912	2-D	yes
2000	CW	100	4, 085	70911	2-D	yes
2000	CW	125	3, 470	42420	2-D	yes
2000	CW	150	3, 754	42419	2-D	yes
2000	CW	175	17, 400	42418	2-D	no
2000	CW	200	22, 106	42417	2-D	no
2400	CW	175	5, 445	42416	2-D	yes
2400	CW	200	8, 352	42415	2-D	yes
2400	CW	225	10, 826	42414	3-D	no
2400	CW	250	19, 988	42413	3-D	no
2400	CW	300	33, 315	42412	3-D	no
2400	CW	400	81, 257	42411	3-D	no
2400	CW	500	92, 745	42410	3-D	no
2400	CW	600	102, 979	42409	3-D	no
2680	CW	175	5, 974	42408	2-D	yes
2680	CW	200	3, 452	42407	2-D	yes
2680	CW	225	11, 807	42406	2-D	no
2680	CW	250	15, 183	42405	3-D	no
2680	CW	300	29, 517	42404	3-D	no
2680	CW	400	47, 742	42403	3-D	no
2680	CW	500	70, 841	42402	3-D	no
2680	CW	600	78, 712	42401	3-D	no

a. Pulse on time/total pulse period
b. Relative plate thickness 2-D or 3-D heat flow.
c. in./min × 0.423 = mm/s.

welding processes. Larger beta grain size promotes lower fracture toughness (Ref. 3). The equiaxed alpha grain structure of the UBM cannot be reformed in the HAZ or FZ without mechanical working in the upper alpha phase field.

Previous research by Mascorella (Ref. 2) indicates that welds exhibiting faster cooling rates than 200°C/s such as those attributed to CO_2 laser welding have softer microstructures than those of typical arc welds. Because of the extremely high rates of cooling known to accompany laser welding, this program of research was conducted to determine the effects of CO_2 laser welding on the microstructure and mechanical properties of Ti-1421. The major objective of this study was to evaluate the CO_2 laser welding variables and their effects on the microstructural and mechanical properties of Ti-1421 welds.

Ti_3Al-Nb Alloy Properties and Physical Metallurgy

Ti_3Al, which is also known as alpha-two (a_2) titanium-aluminide, is an ordered intermetallic compound with a room-temperature hexagonal close-packed (HCP) crystalline structure (Refs. 4–6). Ti_3Al exhibits very low ductility, which can be improved by adding a beta stabilizer such as niobium (Ref. 7). The Ti_3Al-Nb alloy used in this research contained 14.8 wt-% aluminum (25.9 at.-%) and 21.3 wt-% niobium (10.8 at.-%). The Nb content of this alloy is just enough to lower the martensitic start point (M_s) to below room temperature during rapid cooling (Ref. 8).

The beta to a_2 transition temperature of this alloy is suppressed to 1135°C (2075°F) by the Nb addition. Most CO_2 laser welds exhibit high enough cooling rates that an ordered metastable beta DO_{19} superlattice, designated as B_2, is retained at room temperature (Ref. 7).

The macro and microstructure of Ti_3Al-Nb alloy is very dependent on cooling rate. During the weld heating cycle, the material adjacent to the fusion zone that exceeds the beta transus temperature is reverted to beta and may undergo grain growth. The cooling rate determines the maximum size of the beta grains. A low cooling rate process such as gas tungsten arc welding (GTAW) produces larger grain growth than a rapid cooling rate process such as LBW. The beta grains in the HAZ provide sites for epitaxial growth and thus partially dictate the columnar beta grain size in the FZ (Ref. 9). A large beta grain size in the FZ promotes low tensile ductility and preferential paths for crack propagation (Ref. 10).

The property changes in Ti-1421 are determined by the resulting transformation products in the HAZ-FZ. Very slow cooling rates promote the formation of softer transformation products such as Widmanstätten a_2 + beta or colony a_2 + B_2. Intermediate cooling rates produce a mixture of fine acicular a_2 and martensite in a retained beta matrix (Ref. 2). Most arc welding processes have cooling rates within this intermediate range. Rapid cooling rates produce an ordered metastable B_2 microstructure with occasional fine a_2 precipitation at the B_2 grain boundaries (Ref. 7). Thus, at very rapid cooling rates, a more ductile structure than that produced by conventional arc welding can be achieved.

The available literature leads one to conclude that a low heat input joining process that exhibits rapid cooling rates in the FZ/HAZ should produce welds with a microstructure which promotes acceptable room-temperature ductility.

Objectives

The objectives of this investigation were to determine the effects of CO_2 laser welding variables including power and travel speed on the microstructure, microhardness, bend ductility, and fractography of Ti-1421 welds.

Experimental Methods

Materials

The Ti-1421 material used for this study originated from one heat of 1.7-mm (0.067-in.) thick sheet stock, alpha-beta processed from a cast ingot and subsequently surface ground perpendicular to the rolling direction. The chemistry of this material can be found in Table 1. The microstructure of the as-received sheet material is shown in Fig. 1.

CO_2 Laser Beam Welding

A Coherent General EFA-M53 CO_2 industrial laser was used for all laser processing. The M53 laser is a fast axial flow type rated at 2.5 kW of laser power at a 100% duty cycle, but can produce up to 3 kW for short periods of time.

The work chamber consisted of a Lumonics Laserdyne Model 410 CNC machining center which moved the workpiece under the stationary laser beam. For welding, the laser beam was focused through a 127-mm (5-in.) focal length ZnSe lens.

Welding Variable Selection

A series of autogenous CO_2 laser welds was made in both continuous wave and pulse modes. The variables that were used are listed in Table 2. The variables within the capabilities of the equipment used in this study were selected based on earlier testing. All welding was performed "bead-on-plate" unless otherwise noted.

The following steps outline the procedures used to prepare all coupons welded in this research:

1. Each test coupon was saw cut or electric discharge machined (EDM) to size.
2. The machined edges of each coupon were wet ground with a 120-grit SiC belt grinder to remove any burrs or edge cracks.
3. All specimens were glass-bead abraded to remove any oxide layers.
4. The specimens were pickled in a solution of 5 vol-% HF, 40 vol-% HNO_3, and 55 vol-% H_2O for two min and subsequently rinsed in hot running water for 5 min.
5. The specimens were rinsed in acetone, dried and stored in sealed plastic bags.
6. Prior to welding, each specimen was cleaned with acetone and then handled only on the edges of the specimen.

Shielding Technique

Titanium is referred to as a reactive metal because it reacts violently with atmospheric O_2 and N_2 at elevated temperatures. In addition, oxygen and nitrogen dissolve interstitially in titanium and greatly increase the strength of the alpha phase at the expense of ductility. Any fusion welding performed on Ti alloys must be performed in a totally inert atmosphere to prevent this contamination. Helium gas was selected for use as a plasma plume suppressant and also served as an effective shielding media. Early welding test using either coaxial shielding alone or coaxial shielding with an auxiliary side shield proved to be inadequate to prevent visible oxygen contamination. Contamination was noted by a straw-to-purple color on the weld surface.

A shielding technique which utilized an encompassing polyethylene bag (Fig. 2) prevented atmospheric contamination as revealed by a silvery weld bead appearance. An argon back shielding was introduced through the coupon mounting fixture. Argon was purged through the fixture for 2 min prior to welding to displace any air in the shielding bag. The shielding bag was sealed loosely around the laser column for controlled gas leakage. Helium was introduced by the coaxial nozzle. The helium flow through the

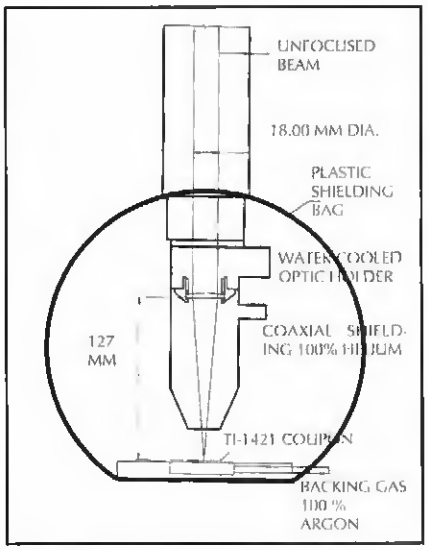

Fig. 2 — Schematic of CO_2 laser setup.

8-mm-diameter (0.314-in) coaxial nozzle was set at approximately 94.3 L/min (200 ft^3/h) (maximum capacity of the flow meter) to insure adequate shielding and to protect the lens from spatter and metal vapor contamination.

Cooling Rate Calculation

As discussed previously, cooling rates could not be measured experimentally due to the rapid heating rates and small heated volume associated with CO_2 laser welds. A common baseline was required to compare the observed experimental data with the laser welding variables. Cooling rate equations developed by Adams (Ref. 11) for arc welding thick and thin plates were used in this research to calculate approximate weld cooling rates. Because both deep and shallow penetration welds were produced in this study, both two- and three-dimension-equations were used.

All cooling rates were estimated using a critical temperature of 880°C (1616°F), the beta to alpha finish temperature. Although the absolute accuracy of the cooling rate calculation is approximately ± 20%, any error is consistent throughout the range of cooling rates in this investigation.

The rapid heat transfer in LBW precludes the use of acceptable preheat temperatures to produce ductile microstructures. Using the 2-D cooling rate equation for a 1000-W weld at 21 mm/s (50 in./min) yields a cooling rate of 2800° to 3000°C/s. A preheat of 775°C (1427°F) is required to lower the cooling rate to an acceptable value of 5°C/s for hardness reduction based on Mascorella's (Ref .2) work.

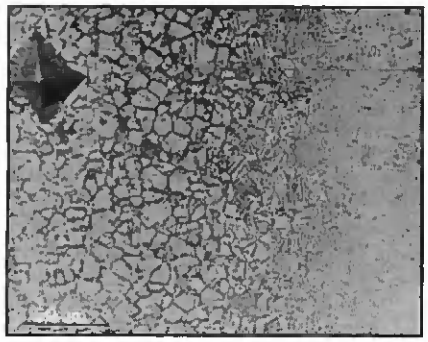

Fig. 3 — Light micrograph of UBM-HAZ boundary of a weld made with 650 W CW and a travel speed of 4.23 mm/s (calculated cooling rate of 195°C/s). Indent at right is approximately 50 μm across.

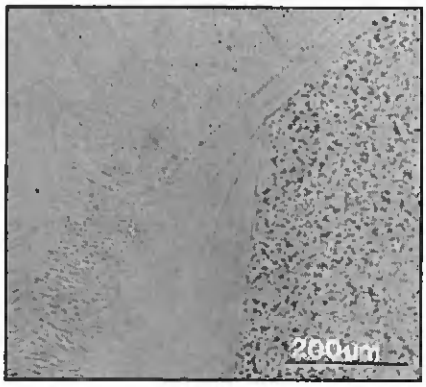

Fig. 4 — Light micrograph of a weld cooled at 5450°C/s, 2400 W CW, 70.1 mm/s. Note beta grain boundaries and solute banding.

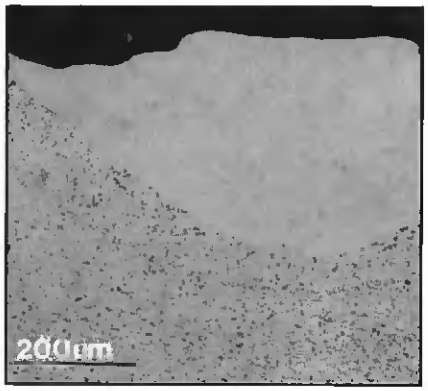

Fig. 5 — Light micrograph of a weld cooled at 20,000°C/s, 2.4 kW CW, 106 mm/s.

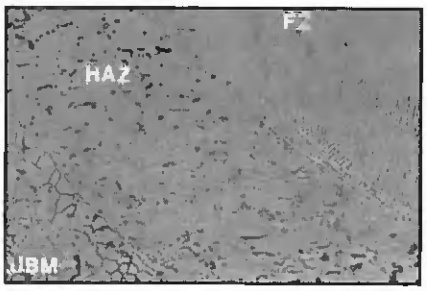

Fig. 6 — Light micrograph of the UBM-HAZ-FZ of a weld cooled at 41,250°C/s, 1 kW, 84.7 mm/s.

Weld Specimen Preparation

Test welds for microhardness evaluation were typically made in groups of 2 to 8 welds per coupon and were 19.05 to 25.4 mm (0.75 to 1.0 in.) in length. The welds were sectioned transversely at the midpoint and polished for microhardness evaluation. The specimens were subsequently etched using Kroll's reagent (1–3 vol-% HF, 4–6 vol-% HNO_3, and balance H_2O)

Microstructure Characterization

Metallography was performed on several of the microhardness test specimens using a light microscope. Optical metallography was conducted up to 400X.

Microhardness Testing

Vickers microhardness testing was accomplished using a 400-g load. The small size of the laser welds limited the nubmer of microhardness indentations made on a single weld. Two indentations were made in the UBM, HAZ and FZ, with one indentation in the FZ center. The indentations in the HAZ were made just inside the HAZ-UBM boundary (far HAZ) and just before the HAZ-FZ boundary (near HAZ).

Bend Testing

Longitudinal three-point face bend tests were conducted on longitudinal weld oriented specimens using a progressively reduced radius slow bending technique. The test was performed by forcing a 12.7 x 50.8 mm (0.5 x 2.0 in.) longitudinally welded specimen to conform to several sizes of radius blocks. A 50.8-mm (2.0-in.) die block was used as the starting radius. A progressively smaller radius was used until the specimen cracked or fractured. The face surface of each specimen was longitudinally ground to a 125-μin. finish to eliminate any stress risers from the weld bead. The elongation was calculated by the following equation:

$$E = (T/2R + T) \times 100 \qquad (1)$$

Where E = strain in %, T = specimen thickness, R = radius of testing block.

The elongation was determined to be the smallest radius block before failure. Three samples were prepared for each condition and averaged for that condition. If a sample broke outside of the radius, the value was discarded.

Longitudinal specimens were used because the bending equipment forced the specimen into an open V block in order to accommodate all of the larger die sizes. A transverse welded specimen would not have conformed to the die radius due to the strength differential transverse to the weldment. Thus an accurate elongation reading could not have been obtained using transverse welded specimens.

Fractography

Scanning electron microscope (SEM) fractography was conducted on several representative fractures. Several UBM bend fracture specimens were also examined for comparative evaluation.

Results and Discussion

Microstructure

Transverse microstructures of the hardness test welds are shown in Figs. 3–7. A light micrograph of the HAZ boundary of a weld made at a power of 650 W CW and a travel speed of 4.23 mm/s (10 in./min) (calculate cooling rate of 195°C/s) is shown with two DPH hardness indents for reference in Fig. 3. Faster travel speeds produced beta grain boundaries with solid-state transformation masking (Fig. 4, 2400 W CW, 70.1 mm/s (175 in./min), 5450°C/s), as well as a centerline solidification pattern and solute banding.

Partial penetration welds with higher calculated cooling rates produced fusion zones consisting mostly of a featureless metastable beta (B2). A shallow penetration mode weld (2.4 kW CW, 106 mm/s (250 in./min), 20,000 °C/s) shown in Fig. 5. The HAZ of this weld is barely discernible. The narrow HAZ and FZ boundary of another shallow penetration weld (1 kW, 84.7 mm/s (200 in./min), 41,200°C/s) are shown in Fig. 6.

Microhardness

The three transverse microhardness plots shown in Figs. 7–9 represent the slowest, an intermediate value, and the fastest cooling rates, respectively. Average HAZ and FZ hardness vs. calculated cooling rate is shown in Fig. 10. Mascorella's GTAW data are included as the lowest five cooling rates for comparison. The GTAW welds have progressively higher microhardness values with increasing cooling rate (from 297 to 488 HAZ and from 292 to 459 FZ for cooling rates from 2 to 50 °C/s). Laser welding with calculated cooling rates between 195° and 10,400 °C/s produced relatively constant microhardness values. These values ranged between 373 and 432 DPH for the HAZ, and between 364

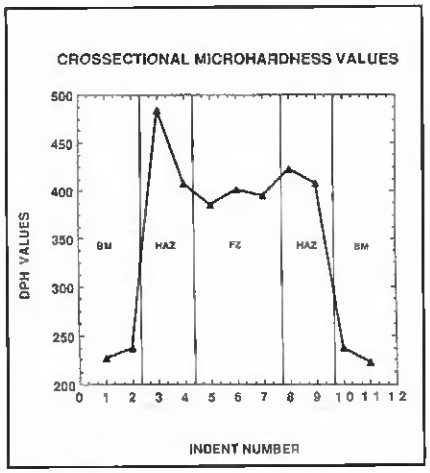

Fig. 7 — Transverse microhardness plot of a weld which was produced with 650 W of CW CO2 laser power at 4.23 mm/s of travel speed and exhibited a cooling rate of 195°C/s.

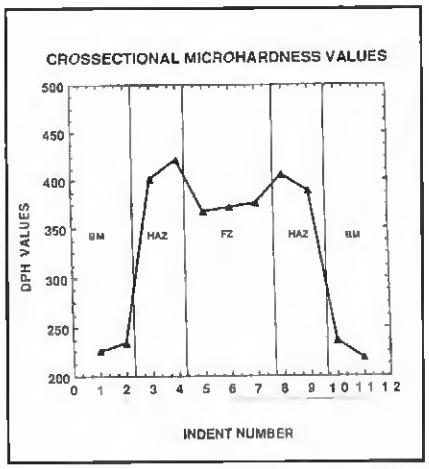

Fig. 8 — Transverse microhardness plot of a weld which was produced with 1400 W of CW CO2 laser power at 69.5 mm/s of travel speed and exhibited a cooling rate of 6560°C/s.

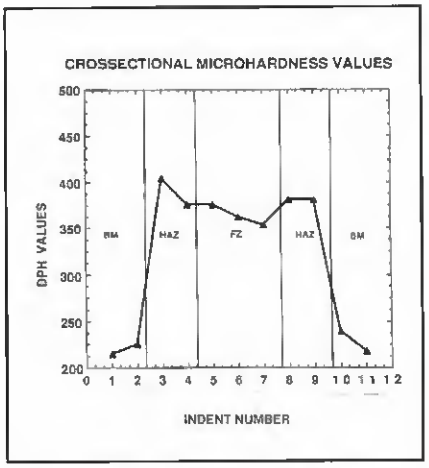

Fig. 9 — Transverse microhardness plot of a weld which was produced with 2400 W of CW CO2 laser power at 211.7 mm/s of travel speed and exhibited a cooling rate of 92,700°C/s.

and 416 for the FZ, and were somewhat lower than the more rapidly cooled GTA welds.

Nearly all of the welds evaluated for microhardness exhibited a higher hardness in the HAZ than in the FZ. One of the possible explanations for this phenomena is the migration of Nb that can occur in the HAZ during cooling. This segregation is not as apparent in the FZ because of the stirring and higher temperature that aides Nb diffusion. Since a decrease of Nb raises the martensitic start temperature, any area that has been depleted of Nb will have a greater tendency to form martensite. This depletion occurs because the beta grains consume the alpha grains in the HAZ upon heating and dissolve the Nb. During cooling, the kinetics are so fast that the Nb cannot diffuse to the newly formed alpha. This newly formed alpha will have a lower Nb content than the nominal composition and will be more susceptible to martensitic formation.

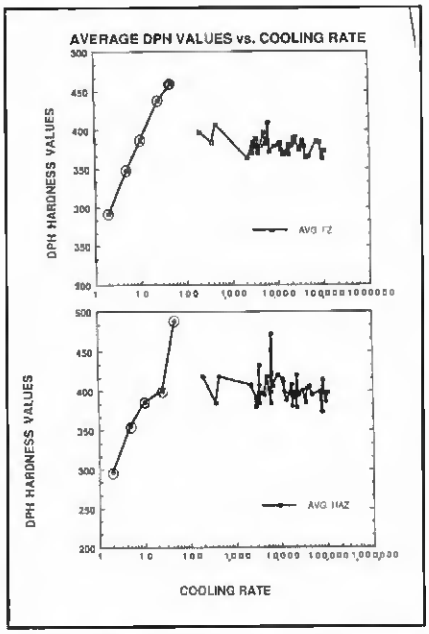

Fig. 10 — Plots of HAZ and FZ microhardness values vs. cooling rate. Circled points denote Mascorella's (Ref. 2) data for GTA welds.

Bend Ductility

The UBM ductility ranged from 2.15 to 3.63%. The laser welded specimens exhibited ductility values from 0.99 to 3.15%. The ductility values are plotted with respect to cooling rate in Fig. 11. The plot reveals that cooling rates of 195°, 451° and 1380°C/s produced welds with bend ductility below the UBM range. Cooling rates of 3470°C/s produced the maximum ductility (2.46 to 3.15%). All of the welds at or above 3470°C/s has bend ductilities within the UBM bend ductility range.

The ductility data for laser welds made with more rapid cooling rates tends to support the hypothesis that the formation of a soft retained metastable B2 in the matrix of the FZ-HAZ produces a more ductile microstructure.

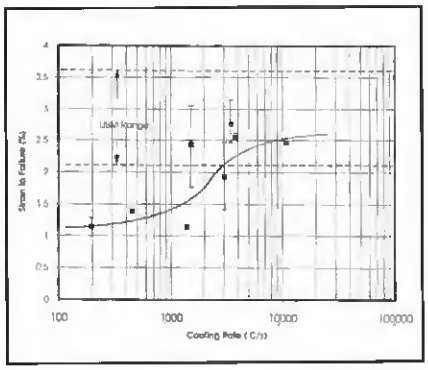

Fig. 11 — Plot of bend ductility vs. cooling rate.

Fractography

SEM fractography for slowly cooled welds with low-bend ductility (Fig. 12, 1 kW CW, 10.6 mm/s (25 in./min), 451°C/s) revealed a macroscopically large, flat, transgranular appearance. More rapidly cooled welds with bend ductilities within the UBM range exhibited a finer, transgranular appearance (Fig. 13, 2 kW CW, 52.9 mm/s (125 in./min)). The presence of a softer retained B2 phase in the matrix of the FZ-HAZ again may account for the more ductile fractographic appearance.

This investigation demonstrates that full penetration laser welds can be made in 0.067-in.-thick Ti-1421 material that will yield ductility values within the UBM range under a wide range of cooling rate conditions.

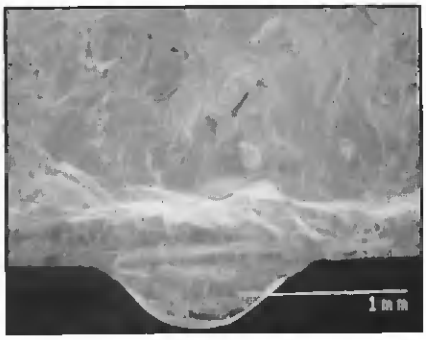

Fig. 12 — SEM fractograph of a weld bend specimen that exhibited a cooling rate of 451°C/s, 1 kW CW, 10.6 mm/s.

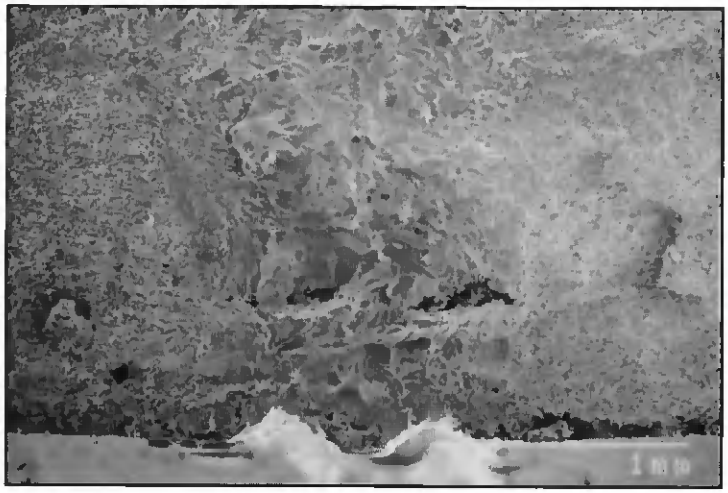

Fig. 13 — SEM fractograph of a weld bend specimen that exhibited a cooling rate of 3470°C/s, 2 kW CW, 52.9 mm/s.

Conclusions

The following conclusions were made as a result of this investigation of CO_2 laser processing of Ti-1421:

1) Macrostructure characterization did not reveal any cracks, porosity or other discontinuities. This indicates that high-quality joints are achievable with CO_2 laser welding in Ti 1421.

2) Laser welding with calculated cooling rates between 195° and 10,400°C/s produced relatively constant microhardness values. These values ranged between 373 and 432 DPH for the HAZ, and between 364 and 416 for the FZ. These results are in contrast to Mascorella's results for gas tungsten arc welding. Mascorella's calculated microhardness values have an increasing trend with increased cooling rate (from 297 to 488 HAZ and from 292 to 459 FZ for cooling rates from 2 to 50°C/s)

3) Ductility values within the UBM range were obtained in full penetration longitudinal bend specimens for laser welds with calculated cooling rates above 3400°C/s. For cooling rates of 1380°C/s and lower ductilities were well below the UBM range. The slower cooled welds exhibited a larger flat cleavage fracture area and lower ductility than the rapidly cooled welds.

Acknowledgments

The authors would like to thank William A. Baeslack for his advice and expert knowledge of reactive metal joining, and General Electric Aircraft Engine Business Group for generously supporting this research.

References

1. Lipsitt, H. A. 1984, Titanium aluminides — An overview, High Temperature Ordered Intermetallic Alloys, eds. C. C. Koch, C. T. Liu and N. S. Stoloff, pp. 531–364, Materials Research Society, Pittsburgh, Pa.

2. Mascorella, T. J. 1987. Weldability of a Ti_3Al-Nb Alloy, M.S. thesis, The Ohio State University, Colubmus, Ohio.

3. Baeslack, W. A. ,Becker, F. D., and Froes, F. H. 1984. Advances in Titanium Alloy Welding Metallurgy, *Journal of Metals*, 36(5): 50.

4. Kerrans, R. S. 1984. Deformation in Ti_3Al fatigued at room and elevated temperatures. *Metallurgical Transactions A*, Vol. 15A, pp. 1721–29.

5. Lipsitt, H. A., Shechtman, D., Schafrik, R. E., The deformation and fracture of Ti_3Al at elevated temperatures. *Metallurgical Transactions* Vol. 11A, pp. 1369–75.

6. Martin, P. L., Lipsitt, H. A., Nufifer, N. T., Williams, J. C. 1980. The effects of alloying on the microstructures and properties of Ti_3Al and Ti-Al. *Proceedings of the Fourth International Conference on Titanium*, H. Kimura and O. Isumi, eds.

7. Baeslack, W. A., Cieslak, M. J., and Headley, T. J. 1988. Structures, properties and fracture of pulsed Nd:YAG laser welded Ti-14.8 wt-%-21.3 wt-%Nb. *Scripta Metallurgica*, Vol. 22, pp. 1155–1160.

8. Strychor, R. and Williams, J. C. 1982. Phase transformations in Ti-Al-Nb alloys, *Solid-Solid Phase Transformations*, H. I. Aaronson, D. E. Laughlin, R. F. Sekerka, C. M. Wayman, eds., The Metallurgical Society of AIME, Warrendale, Pa., p. 250.

9. Savage, W. F. 1980. Houdremont Lecture, Portugal.

10. Baeslack, W. A. Becker, F. D., and Froes, F. H. 1984. Advances in titanium alloy welding metallurgy. *Journal of Metals*, 36(5): 50.

11. Adams, C. M. Jr., 1958. Cooling rates and peak temperatures in fusion welding. *Welding Journal*, 37 (5): 210-s to 215-s.